

Topological orbital Hall effect caused by skyrmions and antiferromagnetic skyrmions

Börge Göbel,^{1,*} Lennart Schimpf,¹ and Ingrid Mertig¹

¹*Institut für Physik, Martin-Luther-Universität Halle-Wittenberg, D-06099 Halle (Saale), Germany*

(Dated: October 2, 2024)

Abstract. The topological Hall effect is a hallmark of topologically non-trivial magnetic textures such as magnetic skyrmions. It quantifies the transverse electric current once an electric field is applied and occurs as a consequence of the emergent magnetic field of the skyrmion. Likewise, an orbital magnetization is generated. Here we show that the charge currents are orbital polarized even though the conduction electrons couple to the skyrmion texture via their spin. The topological Hall effect is accompanied by a topological orbital Hall effect even for s electrons without spin-orbit coupling. As we show, antiferromagnetic skyrmions that have a compensated emergent field, exhibit a pure topological orbital Hall conductivity that is not accompanied by charge transport and can be orders of magnitude larger than the topological spin Hall conductivity.

Introduction

Magnetic skyrmions are non-collinear spin textures that possess an innate stability due to their non-trivial real-space topology [1–3]. They have been observed as individual magnetic objects [4–7] that may serve as carriers of information in future storage technologies [5, 6]. At finite temperatures and magnetic fields, they even form periodic lattices [7, 8] with a rather homogeneous topological charge density n_{Sk} .

This topological charge density has been identified with an effective magnetic field $\mathbf{B}_{\text{em}} \propto n_{\text{Sk}}\mathbf{e}_z$, called ‘emergent field’ [3, 9] that affects the conduction electrons by changing the phase of the wave function; a Berry phase is accumulated [10, 11]. While the electron spins align with the skyrmion texture, an effective Lorentz force acts on their charges and leads to the emergence of transverse transport phenomena: The topological Hall effect [12–14] describes the emergence of a transverse charge current once an electric field is applied. It is the hallmark of the skyrmion crystal phase and the magnitude of its resistivity can be used to measure the skyrmion and topological charge density [15–17]. Since the spins align with the skyrmion texture, the currents are also spin polarized and a topological spin Hall conductivity has been predicted [18–20]. When two skyrmions with opposite topological charges are coupled to form an antiferromagnetic skyrmion [21–26], the topological spin Hall effect is still present but it is not anymore accompanied by charge transport [24, 27].

Different types of skyrmions have been observed on several different length scales [28] and even nano-sized skyrmions can be stabilized [8, 29]. In this case, the emergent field has a magnitude of several thousand Tesla. As a consequence, quantized transport effects occur [30–32] akin to the quantum Hall effect in the presence of a large magnetic field [33–39]. In fact, if the coupling between conduction electron spins and the skyrmion texture is strong, the system can be mapped to a quantum Hall system [30–32] and Landau levels occur giving rise to edge states in the form of skipping orbits.

Over the recent years, the orbital degree of freedom has become increasingly relevant in the field of spinorbitronics, manifesting itself in phenomena such as orbital magnetiza-

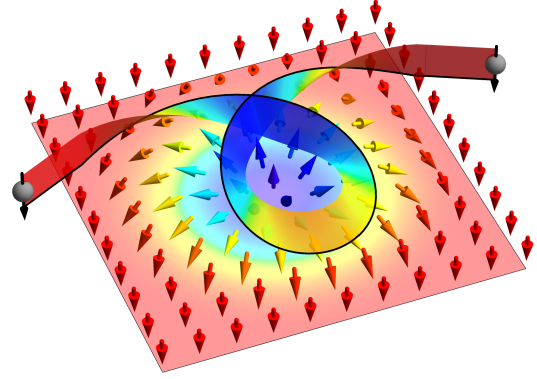


FIG. 1. **Topological orbital Hall effect.** The spin of the conduction electron (black) aligns with the skyrmion texture (colored arrows; the color resembles the out-of-plane orientation). While moving through the skyrmion, the electron accumulates a Berry phase and is deflected (topological Hall effect). Due to the cycloid trajectory (black), an orbital angular momentum is generated and transported as an orbital current (topological orbital Hall effect).

tion [40–45], orbital torque [46, 47], orbital Edelstein effect [48, 49] and orbital Hall effect [50–67]. In the presence of a magnetic field, charge currents form circular trajectories and generate an orbital angular momentum that can be calculated via the modern formulation of orbital magnetization [40–45]. This orbital magnetization has been considered for quantum Hall systems as well as skyrmions [45, 68, 69]. Recently, we have shown that the skipping orbits in quantum Hall systems lead to orbital polarized edge currents [67] that give rise to an orbital Hall effect accompanying the (charge) Hall effect once a transverse electric field is applied.

In this paper, we show that skyrmions give rise to a topological orbital Hall effect (Fig. 1). The orbital currents appear additionally to the topological (charge) Hall effect giving rise to transverse orbital polarized currents. By using a tight-binding model and a Berry curvature approach, we systematically compare the charge, spin and orbital Hall conductivities. Furthermore, we analyze the edge states that occur when the skyrmion is on the nanometer scale. In this scenario the emergent field of the skyrmion is extremely large and Landau levels form. As we show, when two oppositely magnetized skyrmions are coupled to form an

* Correspondence email address: boerge.goebel@physik.uni-halle.de

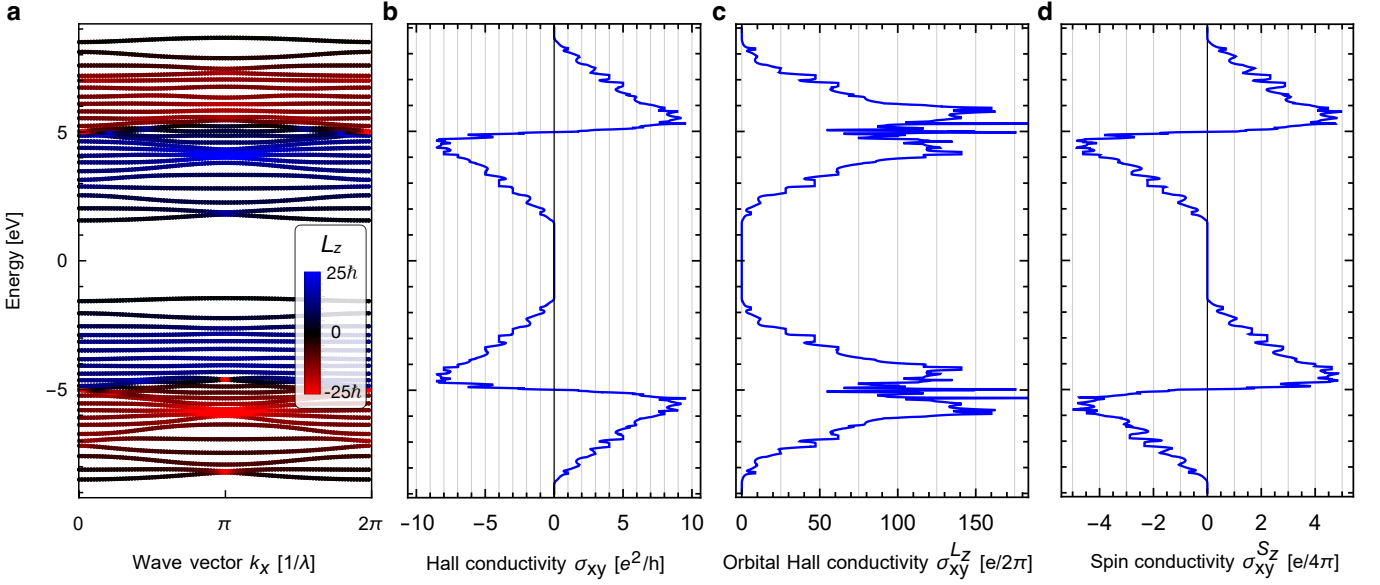


FIG. 2. **Electronic transport in skyrmion crystals.** **a** Band structure $E_{\nu\mathbf{k}}$. The color code indicates the \mathbf{k} - and band-resolved out-of-plane orbital angular momentum $L_{z,\nu}(\mathbf{k})$ (blue: positive, red: negative). The band structure consists of 2 blocks corresponding to parallel and anti-parallel spin alignment. **b** Hall conductivity σ_{xy} as a function of energy. It is quantized in units of e^2/h in the band gaps. **c** Orbital Hall conductivity $\sigma_{xy}^{L_z}$ as a function of energy. **d** Spin Hall conductivity $\sigma_{xy}^{S_z}$ as a function of energy. These calculations correspond to a skyrmion size of $\lambda = 5a$, and a Hund's coupling of $m = 5|t| = 5 \text{ eV}$.

antiferromagnetic skyrmion, the topological Hall effect is compensated and only orbital and spin Hall effects emerge. Since the orbital angular momentum of a skyrmion can be arbitrarily high, the topological orbital Hall conductivity can be orders of magnitude larger than the topological spin Hall conductivity.

Results and discussion

Spinorbitronic transport in non-collinear spin textures.

We consider a square lattice with lattice constant a and a single s orbital per site for the conduction electrons. The skyrmion texture is a rotational symmetric vector field $\mathbf{m}(\mathbf{r})$ (normalized) with diameter λ which is shown in Fig. 1 (for details see Methods section) that is formed by energetically lower lying d electrons. The non-collinear texture increases the magnetic unit cell to $\lambda \times \lambda$ lattice sites.

The s - d Hamiltonian consists of a nearest-neighbor hopping term (amplitude $t = -1 \text{ eV}$) and a Hund's coupling term (quantified by m)

$$H = \sum_{\langle ij \rangle} t c_i^\dagger c_j + m \sum_i \mathbf{m}_i \cdot (c_i^\dagger \boldsymbol{\sigma} c_i). \quad (1)$$

c_i^\dagger and c_i are the creation and annihilation operators at site i . $\boldsymbol{\sigma}$ is the vector of the Pauli matrices characterizing the spin of the conduction electrons. The eigenvalues $E_{\nu\mathbf{k}}$ are the band structure (band index ν and wave vector \mathbf{k}) and the eigenvectors $|\nu\mathbf{k}\rangle$ will be used to determine the observables discussed in this paper: Spin $S_{\nu,z}(\mathbf{k})$ and orbital angular momentum $L_{\nu,z}(\mathbf{k})$, as well as the charge Hall conductivity $\sigma_{xy}(E_F)$, spin Hall conductivity $\sigma_{xy}^{S_z}(E_F)$ and orbital Hall conductivity $\sigma_{xy}^{L_z}(E_F)$ that are calculated as integrals over the Berry curva-

ture $\Omega_{\nu,z}(\mathbf{k})$, spin Berry curvature $\Omega_{\nu,z}^{S_z}(\mathbf{k})$ and orbital Berry curvature $\Omega_{\nu,z}^{L_z}(\mathbf{k})$ over the Brillouin zone as functions of the Fermi energy E_F . For more details about the calculations, we refer to the Methods section.

Band structure, orbital and spin angular momentum in skyrmion textures. The band structure $E_{\nu\mathbf{k}}$ depends on the strength of the Hund's coupling m . Starting the discussion from $m = 0$, all bands are spin degenerate and the band structure resembles the single tight-binding band of the square lattice $E(\mathbf{k}) = 2t[\cos(k_x a) + \cos(k_y a)]$ but backfolded into the smaller magnetic Brillouin zone accounting for the skyrmion. Upon increasing m , the electron spins start to align with the skyrmion texture and the initially spin-degenerate bands start to split. The band structure for $m = 1 \text{ eV} = |t|$ exhibits many (avoided) band crossings and is shown in Fig. S1 of the Supplementary Material.

Once the coupling m is larger than the initial band width $4|t|$, the spins are almost completely aligned with the skyrmion. Two blocks emerge – one for parallel spin alignment and one for antiparallel spin alignment – shifted by $\pm m$, respectively. Results for $m = 5 \text{ eV} = 5|t|$ are shown in Fig. 2(a). The bands in the two blocks are similar and have a weak dispersion. In the limit of strong Hund's coupling and large skyrmion sizes, the two blocks become completely equivalent. In this adiabatic limit, the bands are Landau levels akin to the bands of a quantum Hall system. In Refs. [20, 31, 32], we have shown that the Hamiltonian hosting the non-collinear skyrmion texture can be transformed to a quantum Hall Hamiltonian with a collinear magnetic field coupling to the charge of the electrons. This magnetic field is the 'emergent field' \mathbf{B}_{em} mentioned in the introduction.

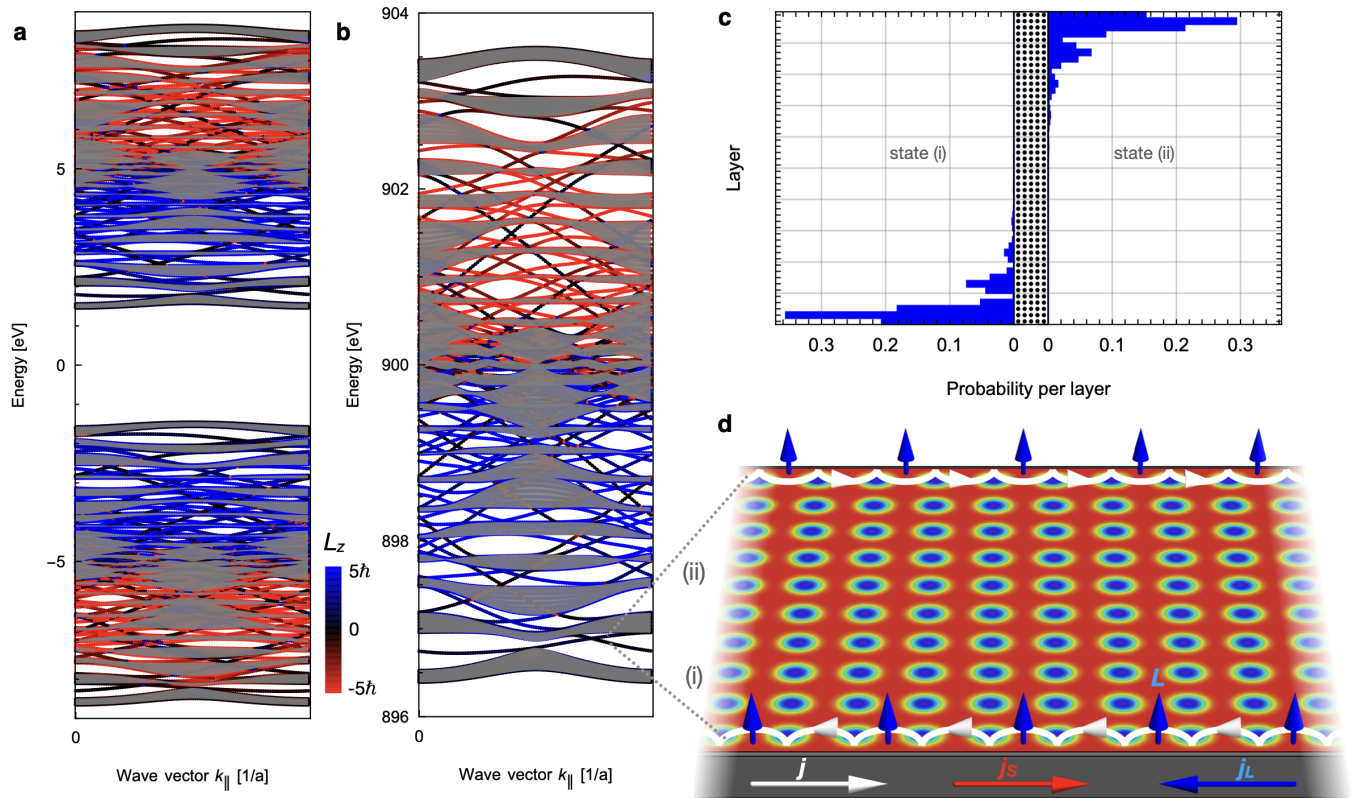


FIG. 3. **Edge states carrying orbital angular momentum.** **a** Band structure of a slab with 10 skyrmions in the unit cell. The color indicates the orbital angular momentum (see legend). Gray areas indicate bulk states, projected from the bulk band structure (cf. Fig. 2a). These calculations correspond to a skyrmion size of $\lambda = 5a$, and a Hund's coupling of $m = 5|t| = 5 \text{ eV}$. **b** Zoom of the upper block for $m = 900|t| = 900 \text{ eV}$ corresponding to the adiabatic limit of very strong coupling. **c** Layer-resolved probability of the two edge states highlighted in **b**, indicated as (i) and (ii). The unit cell is indicated in the middle. **d** Schematic visualization of the two edge states giving rise to charge currents \mathbf{j} , spin currents \mathbf{j}_S and orbital currents \mathbf{j}_L that are oriented oppositely at both edges.

While the two blocks in the band structure are characterized by opposite spin alignment, that is rather homogeneous within a block ($s_{\nu,z}(\mathbf{k}) \approx \pm \hbar/2 \langle m_z \rangle$ with $\langle m_z \rangle$ the average out-of-plane magnetic moment of the skyrmion), the orbital angular momentum $L_{\nu,z}(\mathbf{k})$ is also roughly opposite comparing the two blocks but changes within a block. We have added it as a color code to Fig. 2(a). Starting from the lowest band, it is negative and increases in magnitude until it changes sign near $E = -m = -5 \text{ eV}$ and decreases back to zero. Its magnitude is much larger than the spin by multiple \hbar (cf. legend in Fig. 2a).

Topological charge, spin and orbital Hall effect. The analogy of the considered skyrmion system and a quantum Hall system allows to understand the emergence of a topological Hall effect, as discussed in Refs. [31, 32]. Since the bands are (at least partially) spin polarized, the corresponding currents are spin polarized, as discussed in Ref. [20]. Therefore, a topological spin Hall conductivity occurs as well. As we have just shown, the bands are also orbital polarized, so the emergence of a topological orbital Hall conductivity is expected as well. The energy dependent curves of the Hall conductivity σ_{xy} , orbital Hall conductivity $\sigma_{xy}^{L_z}$ and spin Hall conductivity $\sigma_{xy}^{S_z}$ are shown in Fig. 2(b-d), respectively.

First, and most importantly, the orbital Hall conductivity

(panel c) is non-zero. This means, a skyrmion exhibits orbital and spin polarized currents; a topological orbital Hall effect is superimposed on top of the previously observed topological Hall and topological spin Hall effects.

Since the electron spins align parallel with the skyrmion in the lower block of the band structure and antiparallel in the upper block, we see also two Blocks in the conductivities. For the topological Hall effect (b), the signals are roughly reversed, because the parallel and antiparallel alignment corresponds to an interaction with oppositely oriented emergent fields $\mathbf{B}_{\text{em}} \parallel \pm e_z$ of the skyrmion. The orbital (c) and spin Hall conductivities (d) exhibit almost the same signals comparing the two blocks because reversing the alignment of the spins with the skyrmion texture, does not only reverse the emergent field but also S_z and L_z .

Within a Block, the topological Hall conductivity (b) and spin Hall conductivity change sign (d). This is because the electrons in the lower half of a block are characterized by a positive effective mass and in the upper half by a negative effective mass (hole-like behavior) which is determined by the band structure of the square lattice $E(\mathbf{k}) = 2t[\cos(k_x a) + \cos(k_y a)] \pm m$. Particles of opposite mass are deflected into opposite directions by the same emergent magnetic field. However, by changing the sign of the effective mass, L_z

changes sign as well, as in classical physics $\mathbf{L} = m\mathbf{r} \times \dot{\mathbf{r}}$. For this reason, the orbital Hall conductivity (c) remains always positive.

The orbital Hall conductivity (c) surpasses the spin Hall conductivity (d) by more than an order of magnitude because L_z can in principle have arbitrarily high values while S_z is limited by $\pm\hbar/2$. Both orbital (c) and spin Hall conductivities (d) can exhibit plateaus, e. g. between the two Landau levels near $E = 3\text{ eV}$. However, the values are not quantized by a natural constant, because spin and orbital angular momentum are no good quantum numbers in the skyrmion system. The topological Hall conductivity (b) on the other hand is quantized in units of e^2/h due to the mathematical equivalence to a quantum Hall system.

Edge states. By considering a slab geometry, we gain information about edge states contributing to the different transverse transport phenomena. We repeat the skyrmion unit cell 10 times along the y direction and keep periodicity along the x direction. The corresponding band structure is shown in Fig. 3a. Additionally, we have superimposed $L_{\nu,z}(k_{\parallel})$ as a color code (red and blue) and the projected bulk bands in gray. Edge states are present that bridge the gaps between the bulk states. As the main result, they are orbital and spin polarized.

The discussion becomes easier if we are in the adiabatic limit where $m \gg |t|$. Therefore, Fig. 3b shows the upper block for $m = 900|t| = 900\text{ eV}$. Similar to the Landau levels appearing in the bulk, the edge states are orbital polarized explaining the origin of the orbital Hall conductivity. In the gap between the lowest two bands in the upper block, we observe two states labeled (i) and (ii). Fig. 3c shows that they are located at opposite edges of the slab. Their orbital angular momentum is positive and the spin and charge are negative. This corresponds to the positive orbital Hall conductivity and negative topological Hall and spin Hall conductivities calculated for the bulk at that energy. A schematic interpretation in terms of skipping orbits is shown in Fig. 3d: By combining a translational and rotational degree of freedom, orbital angular momentum is transported along the edge as an orbital current.

Different types of skyrmions. The above discussed calculations can be repeated for other non-collinear spin textures related to skyrmions [28]. We start by discussing other objects with a finite topological charge. To classify such objects, one can introduce the topological charge $N_{\text{Sk}} = pv$ that is the product of polarity $p = \pm 1$ (out-of-plane orientation of the center magnetic moment) and vorticity $v = 0, \pm 1, \pm 2, \dots$. The latter quantity relates the polar angle of the position vector φ with the polar angle of the magnetic texture ϕ via $\phi = v\varphi + \gamma$. Here, γ is an offset that is called helicity. Since the topological charge is independent of the helicity, Néel ($\gamma = 0, \pi$) and Bloch skyrmions ($\gamma = \pm\pi/2$) of otherwise equal profile and electronic properties exhibit the same topological Hall, spin Hall and orbital Hall responses.

So far, we have discussed skyrmions that are characterized by $p = 1$ and $v = 1$ so that they carry a topological charge of $N_{\text{Sk}} = +1$. As a consequence, their emergent field for parallel spin-alignment points along $+z$. If we consider the same skyrmions in a ferromagnetic background that is oriented oppositely, the polarity changes sign $p = -1$ and so does the

topological charge $N_{\text{Sk}} = -1$. As a consequence, the emergent field points along $-z$ and so the topological Hall conductivity changes sign. However, the spin Hall conductivity and the orbital Hall conductivity remain invariant because S_z and L_z change sign as well, due to the reversed skyrmion texture and emergent field, respectively.

A similar discussion holds for antiskyrmions [70] that are characterized by a negative vorticity $v = -1$. Antiskyrmions and skyrmions in the same magnetic background (same polarity p) have opposite topological charges and therefore opposite emergent fields. As a consequence, they exhibit opposite topological Hall conductivities but the same spin and orbital Hall conductivities. If skyrmions and antiskyrmions coexist at equal numbers, as is possible in frustrated magnets [29] or Heusler materials [71–74], the net topological Hall conductivity is compensated but the spin and orbital Hall effects are not which makes the latter two effects ideal to detect topological magnetic textures if one is not sure about the type of texture.

The idea of coupling two skyrmionic textures with opposite topological charges gave rise to other textures such as the skyrmionium [75–77] or the antiferromagnetic skyrmion [21–26]. In the following, we will discuss the case of the antiferromagnetic skyrmion in detail.

Pure topological orbital Hall effect in antiferromagnetic skyrmions. To model an antiferromagnetic skyrmion, we take the texture considered before and reverse every second magnetic moment in a checkerboard pattern (cf. Fig. 4a). This allows to distinguish two skyrmions on two sublattices with opposite magnetic moments and topological charges leading to a compensated topological charge overall.

Besides this true antiferromagnetic skyrmion [21, 23, 24], synthetic antiferromagnetic skyrmions (cf. Fig. 4b) have been considered as well [22, 25, 26]. In the latter case, the interpretation of two coexisting sub-skyrmions is even more applicable. This is especially true once we extend the sd-Hamiltonian to first and second nearest neighbor hopping and consider only second-nearest neighbor hopping t_2 .

The corresponding charge, orbital and spin Hall conductivities for $t_1 = 0$ and $t_2 = -1\text{ eV}$ are shown in Fig. 4c-e. The bands are doubly degenerate resembling the opposite spin alignment in the two sublattices hosting skyrmions with opposite emergent magnetic fields. As a consequence, the topological Hall effect is compensated for every energy (Fig. 4c) but the orbital and spin Hall conductivities are finite (Fig. 4d,e). Their energy dependencies are similar to those of the conventional skyrmion presented in Fig. 2c,d but their magnitude is larger due to the two coexisting sublattices and the larger skyrmion size. Qualitatively similar results can be obtained for nearest-neighbor hopping only ($t_1 = -1\text{ eV}$ and $t_2 = 0$, presented in Fig. S2d-f of the Supplementary Material) and both hoppings considered ($t_1 = -2/3\text{ eV}$ and $t_2 = -2/3\text{ eV}$, presented in Fig. S2a-c of the Supplementary Material).

Independent of the choice of hopping amplitudes, a pure Hall effect of angular momentum (orbital and spin) emerges while the charge transport is compensated. The precise energy dependence, however, can be very different once the hoppings are modified because the electronic structure changes.

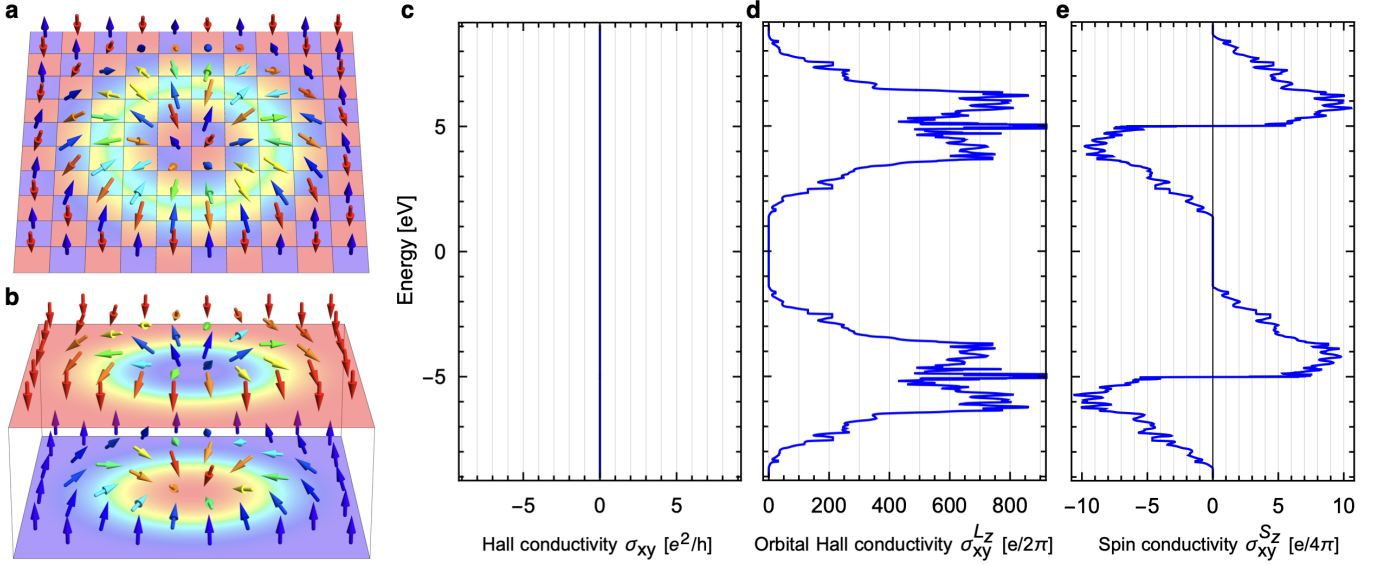


FIG. 4. **Pure topological orbital Hall effect in antiferromagnetic skyrmion crystals.** **a** Antiferromagnetic skyrmion in one layer. The color resembles the out-of-plane orientation of the magnetic moments (arrows). **b** Synthetic antiferromagnetic skyrmion in two layers. **c** Hall conductivity σ_{xy} , **d** orbital Hall conductivity σ_{xy}^{Lz} and **e** spin Hall conductivity σ_{xy}^{Sz} as a function of energy in an antiferromagnetic skyrmion crystal characterized by second-nearest neighbor hopping $t_2 = -1$ eV and a Hund's coupling strength of $m = 5$ eV and skyrmion size $\lambda = 8a$.

Conclusions

In summary, we have shown that skyrmions and antiferromagnetic skyrmions give rise to a topological orbital Hall effect. For conventional skyrmions, the net emergent field forces electrons onto circular trajectories and causes skipping orbits at the edges akin to the quantum Hall effect. This gives rise to a topological Hall effect for which the charge currents are spin and orbital polarized. An antiferromagnetic skyrmions on the other hand, consists of two oppositely oriented subskyrmions on two sublattices. The opposite emergent fields cause opposite topological Hall effects and opposite spin and orbital polarization giving rise to a compensated topological Hall effect but net spin and orbital Hall effects.

Since the orbital angular momentum can take arbitrarily high values, the orbital Hall conductivity is much larger than the spin Hall conductivity. The orbital Hall conductivity scales roughly quadratically with the skyrmion diameter while the spin and charge Hall conductivities scale roughly linearly. This means these textures could serve as generators of large orbital currents that can potentially transport information and give rise to considerable orbital torques [46, 47].

The results presented for the skyrmion can be carried over to other topological spin textures such as antiskyrmions [70], bimerons [78–80] and biskyrmions [81, 82]. Likewise, the results of the antiferromagnetic skyrmion can be carried over to other compensated topological spin textures such as skyrmioniums [75–77].

Methods

Skyrmion texture. A skyrmion centered at $\mathbf{r}_0 = 0$ is

modelled by

$$\mathbf{m} = \begin{pmatrix} x \sin(2\pi r/\lambda)/r \\ y \sin(2\pi r/\lambda)/r \\ \cos(2\pi r/\lambda) \end{pmatrix} \quad (2)$$

for $r = \sqrt{x^2 + y^2} < \lambda/2$ and $\mathbf{m} = -\mathbf{e}_z$ otherwise.

Note that this is only an approximation for the normalized skyrmion profile. The precise magnetization profile is determined by the interplay of several magnetic interactions and depends on the magnetic parameters. Most important for our purposes is the topological charge [3]

$$N_{\text{Sk}} = \frac{1}{4\pi} \int_{xy} \mathbf{m}(\mathbf{r}) \cdot \left[\frac{\partial \mathbf{m}(\mathbf{r})}{\partial x} \times \frac{\partial \mathbf{m}(\mathbf{r})}{\partial y} \right] d^2r. \quad (3)$$

which is an integer for the above considered Néel skyrmion, $N_{\text{Sk}} = +1$.

Calculation of the observables. The spin is calculated as

$$S_{z,\nu}(\mathbf{k}) = \frac{\hbar}{2} \langle \nu \mathbf{k} | \sigma_z | \nu \mathbf{k} \rangle. \quad (4)$$

We calculate the orbital angular momentum based on the modern formulation including the off-diagonal elements of the tensor [57, 67]

$$\begin{aligned} \langle \nu \mathbf{k} | L_z | \alpha \mathbf{k} \rangle &= i \frac{e\hbar^2}{4g_L\mu_B} \sum_{\beta \neq \nu, \alpha} \left(\frac{1}{E_{\beta\mathbf{k}} - E_{\nu\mathbf{k}}} + \frac{1}{E_{\beta\mathbf{k}} - E_{\alpha\mathbf{k}}} \right) \\ &\times (\langle \nu \mathbf{k} | v_x | \beta \mathbf{k} \rangle \langle \beta \mathbf{k} | v_y | \alpha \mathbf{k} \rangle - \langle \nu \mathbf{k} | v_y | \beta \mathbf{k} \rangle \langle \beta \mathbf{k} | v_x | \alpha \mathbf{k} \rangle). \end{aligned} \quad (5)$$

Here, $\mathbf{v} = \frac{1}{\hbar}\nabla_{\mathbf{k}}H$ is the velocity operator. $L_{\nu,z}(\mathbf{k})$ are the diagonal elements of the tensor $L_{\nu,z}(\mathbf{k}) = \langle \nu\mathbf{k} | L_z | \nu\mathbf{k} \rangle$.

The intrinsic Hall conductivity [83]

$$\sigma_{xy}(E_F) = -\frac{e^2}{\hbar} \sum_{\nu} \frac{1}{2\pi} \int_{E_{\nu\mathbf{k}} \leq E_F} \Omega_{\nu,z}(\mathbf{k}) d^2k \quad (6)$$

is calculated by integrating the reciprocal space Berry curvature over all occupied states in the Brillouin zone (states below the Fermi energy E_F at zero temperature). The Berry curvature is [10]

$$\Omega_{\nu,z}(\mathbf{k}) = -2\hbar^2 \text{Im} \sum_{\mu \neq \nu} \frac{\langle \nu\mathbf{k} | v_x | \mu\mathbf{k} \rangle \langle \mu\mathbf{k} | v_y | \nu\mathbf{k} \rangle}{(E_{\nu\mathbf{k}} - E_{\mu\mathbf{k}})^2}. \quad (7)$$

The orbital and spin Hall conductivities [57]

$$\sigma_{xy}^{L_z}(E_F) = \frac{e}{\hbar} \sum_{\nu} \frac{1}{(2\pi)^2} \int_{E_{\nu\mathbf{k}} \leq E_F} \Omega_{\nu,z}^{L_z}(\mathbf{k}) d^2k, \quad (8)$$

$$\sigma_{xy}^{S_z}(E_F) = \frac{e}{\hbar} \sum_{\nu} \frac{1}{(2\pi)^2} \int_{E_{\nu\mathbf{k}} \leq E_F} \Omega_{\nu,z}^{S_z}(\mathbf{k}) d^2k \quad (9)$$

are calculated from the orbital and spin Berry curvatures, respectively,

$$\Omega_{\nu,z}^{L_z}(\mathbf{k}) = -2\hbar^2 \text{Im} \sum_{\mu \neq \nu} \frac{\langle \nu\mathbf{k} | j_x^{L_z} | \mu\mathbf{k} \rangle \langle \mu\mathbf{k} | v_y | \nu\mathbf{k} \rangle}{(E_{\nu\mathbf{k}} - E_{\mu\mathbf{k}})^2}, \quad (10)$$

$$\Omega_{\nu,z}^{S_z}(\mathbf{k}) = -2\hbar^2 \text{Im} \sum_{\mu \neq \nu} \frac{\langle \nu\mathbf{k} | j_x^{S_z} | \mu\mathbf{k} \rangle \langle \mu\mathbf{k} | v_y | \nu\mathbf{k} \rangle}{(E_{\nu\mathbf{k}} - E_{\mu\mathbf{k}})^2}, \quad (11)$$

where $\langle \nu\mathbf{k} | j_x^{L_z} | \mu\mathbf{k} \rangle = \frac{1}{2} \sum_{\alpha} [\langle \nu\mathbf{k} | v_x | \alpha\mathbf{k} \rangle \langle \alpha\mathbf{k} | L_z | \mu\mathbf{k} \rangle + \langle \nu\mathbf{k} | L_z | \alpha\mathbf{k} \rangle \langle \alpha\mathbf{k} | v_x | \mu\mathbf{k} \rangle]$ is the orbital current operator and $\langle \nu\mathbf{k} | j_x^{S_z} | \mu\mathbf{k} \rangle = \frac{1}{2} [\langle \nu\mathbf{k} | v_x | \nu\mathbf{k} \rangle \langle \mu\mathbf{k} | S_z | \mu\mathbf{k} \rangle + \langle \nu\mathbf{k} | S_z | \nu\mathbf{k} \rangle \langle \mu\mathbf{k} | v_x | \mu\mathbf{k} \rangle]$ the spin current operator.

Data availability

Data that support the findings of this work are available from the authors on reasonable request.

Code availability

The code that supports the findings of this work is available from the authors on reasonable request.

Acknowledgements

This work was supported by the EIC Pathfinder OPEN grant 101129641 ‘‘Orbital Engineering for Innovative Electronics’’.

Author contributions

B.G. and L.S. performed the calculations. B.G. wrote the manuscript with significant inputs from all authors. B.G. prepared the figures. All authors discussed the results. B.G. planned the project. B.G. and I.M. supervised the project. I.M. provided the funding.

Supplementary information

accompanies this paper at [insert link].

Competing interests

The authors declare no competing interests.

-
- [1] Bogdanov, A. & Yablonskii, D. Thermodynamically stable vortices in magnetically ordered crystals. the mixed state of magnets. *Zh. Eksp. Teor. Fiz* **95**, 182 (1989).
- [2] Mühlbauer, S. *et al.* Skyrmion lattice in a chiral magnet. *Science* **323**, 915–919 (2009).
- [3] Nagaosa, N. & Tokura, Y. Topological properties and dynamics of magnetic skyrmions. *Nature Nanotechnol.* **8**, 899–911 (2013).
- [4] Romming, N. *et al.* Writing and deleting single magnetic skyrmions. *Science* **341**, 636–639 (2013).
- [5] Sampaio, J., Cros, V., Rohart, S., Thiaville, A. & Fert, A. Nucleation, stability and current-induced motion of isolated magnetic skyrmions in nanostructures. *Nature Nanotechnol.* **8**, 839 (2013).
- [6] Fert, A., Cros, V. & Sampaio, J. Skyrmions on the track. *Nature Nanotechnol.* **8**, 152–156 (2013).
- [7] Yu, X. *et al.* Real-space observation of a two-dimensional skyrmion crystal. *Nature* **465**, 901–904 (2010).
- [8] Heinze, S. *et al.* Spontaneous atomic-scale magnetic skyrmion lattice in two dimensions. *Nature Phys.* **7**, 713–718 (2011).
- [9] Schulz, T. *et al.* Emergent electrodynamics of skyrmions in a chiral magnet. *Nature Phys.* **8**, 301–304 (2012).
- [10] Berry, M. V. Quantal phase factors accompanying adiabatic changes. *Proceedings of the Royal Society of London A: Mathematical, Physical and Engineering Sciences* **392**, 45–57 (1984).
- [11] Zak, J. Berry’s phase for energy bands in solids. *Phys. Rev. Lett.* **62**, 2747 (1989).
- [12] Bruno, P., Dugaev, V. & Taillefumier, M. Topological Hall effect and Berry phase in magnetic nanostructures. *Phys. Rev. Lett.* **93**, 096806 (2004).
- [13] Neubauer, A. *et al.* Topological Hall effect in the A phase of MnSi. *Phys. Rev. Lett.* **102**, 186602 (2009).
- [14] Lee, M., Kang, W., Onose, Y., Tokura, Y. & Ong, N. Unusual Hall effect anomaly in MnSi under pressure. *Phys. Rev. Lett.* **102**, 186601 (2009).
- [15] Maccariello, D. *et al.* Electrical detection of single magnetic skyrmions in metallic multilayers at room temperature. *Nature Nanotechnol.* **13**, 233 (2018).
- [16] Sivakumar, P. K. *et al.* Topological Hall signatures of two chiral spin textures hosted in a single tetragonal inverse Heusler thin film. *ACS Nano* **14**, 13463–13469 (2020).
- [17] Raju, M. *et al.* Colossal topological Hall effect at the transition between isolated and lattice-phase interfacial skyrmions. *Nature Comms.* **12**, 2758 (2021).
- [18] Yin, G., Liu, Y., Barlas, Y., Zang, J. & Lake, R. K. Topological spin Hall effect resulting from magnetic skyrmions. *Phys. Rev. B* **92**, 024411 (2015).
- [19] Ndiaye, P. B., Akosa, C. A. & Manchon, A. Topological Hall and spin Hall effects in disordered skyrmionic textures. *Phys. Rev. B* **95**, 064426 (2017).

- [20] Göbel, B., Mook, A., Henk, J. & Mertig, I. The family of topological Hall effects for electrons in skyrmion crystals. *Eur. Phys. J. B* **91**, 179 (2018).
- [21] Barker, J. & Tretiakov, O. A. Static and dynamical properties of antiferromagnetic skyrmions in the presence of applied current and temperature. *Phys. Rev. Lett.* **116**, 147203 (2016).
- [22] Zhang, X., Zhou, Y. & Ezawa, M. Magnetic bilayer-skyrmions without skyrmion Hall effect. *Nature Comms.* **7**, 10293 (2016).
- [23] Zhang, X., Zhou, Y. & Ezawa, M. Antiferromagnetic skyrmion: stability, creation and manipulation. *Sci. Rep.* **6**, 24795 (2016).
- [24] Göbel, B., Mook, A., Henk, J. & Mertig, I. Antiferromagnetic skyrmion crystals: Generation, topological Hall, and topological spin Hall effect. *Phys. Rev. B* **96**, 060406 (2017).
- [25] Legrand, W. *et al.* Room-temperature stabilization of antiferromagnetic skyrmions in synthetic antiferromagnets. *Nature Mater.* **19**, 34–42 (2020).
- [26] Dohi, T., DuttaGupta, S., Fukami, S. & Ohno, H. Formation and current-induced motion of synthetic antiferromagnetic skyrmion bubbles. *Nature Comms.* **10**, 5153 (2019).
- [27] Buhl, P. M., Freimuth, F., Blügel, S. & Mokrousov, Y. Topological spin Hall effect in antiferromagnetic skyrmions. *physica status solidi (RRL)-Rapid Research Letters* **11**, 1700007 (2017).
- [28] Göbel, B., Mertig, I. & Tretiakov, O. A. Beyond skyrmions: Review and perspectives of alternative magnetic quasiparticles. *Physics Reports* **895**, 1–28 (2021).
- [29] Okubo, T., Chung, S. & Kawamura, H. Multiple-q states and the skyrmion lattice of the triangular-lattice heisenberg antiferromagnet under magnetic fields. *Phys. Rev. Lett.* **108**, 017206 (2012).
- [30] Hamamoto, K., Ezawa, M. & Nagaosa, N. Quantized topological Hall effect in skyrmion crystal. *Phys. Rev. B* **92**, 115417 (2015).
- [31] Göbel, B., Mook, A., Henk, J. & Mertig, I. Unconventional topological Hall effect in skyrmion crystals caused by the topology of the lattice. *Phys. Rev. B* **95**, 094413 (2017).
- [32] Göbel, B., Mook, A., Henk, J. & Mertig, I. Signatures of lattice geometry in quantum and topological Hall effect. *New J. Phys.* **19**, 063042 (2017).
- [33] Landau, L. Diamagnetismus der Metalle. *Z. Phys.* **64**, 629–637 (1930).
- [34] Onsager, L. Interpretation of the de Haas-van Alphen effect. *The London, Edinburgh, and Dublin Philosophical Magazine and Journal of Science* **43**, 1006–1008 (1952).
- [35] Hofstadter, D. R. Energy levels and wave functions of Bloch electrons in rational and irrational magnetic fields. *Phys. Rev. B* **14**, 2239 (1976).
- [36] Klitzing, K. v., Dorda, G. & Pepper, M. New method for high-accuracy determination of the fine-structure constant based on quantized Hall resistance. *Phys. Rev. Lett.* **45**, 494 (1980).
- [37] Thouless, D., Kohmoto, M., Nightingale, M. & Den Nijs, M. Quantized Hall conductance in a two-dimensional periodic potential. *Phys. Rev. Lett.* **49**, 405 (1982).
- [38] Hatsugai, Y., Fukui, T. & Aoki, H. Topological analysis of the quantum Hall effect in graphene: Dirac-Fermi transition across van Hove singularities and edge versus bulk quantum numbers. *Phys. Rev. B* **74**, 205414 (2006).
- [39] Sheng, D., Sheng, L. & Weng, Z. Quantum Hall effect in graphene: disorder effect and phase diagram. *Phys. Rev. B* **73**, 233406 (2006).
- [40] Chang, M.-C. & Niu, Q. Berry phase, hyperorbits, and the Hofstadter spectrum: Semiclassical dynamics in magnetic Bloch bands. *Phys. Rev. B* **53**, 7010 (1996).
- [41] Xiao, D., Shi, J. & Niu, Q. Berry phase correction to electron density of states in solids. *Phys. Rev. Lett.* **95**, 137204 (2005).
- [42] Thonhauser, T., Ceresoli, D., Vanderbilt, D. & Resta, R. Orbital magnetization in periodic insulators. *Phys. Rev. Lett.* **95**, 137205 (2005).
- [43] Ceresoli, D., Thonhauser, T., Vanderbilt, D. & Resta, R. Orbital magnetization in crystalline solids: Multi-band insulators, Chern insulators, and metals. *Phys. Rev. B* **74**, 024408 (2006).
- [44] Raoux, A., Piéchon, F., Fuchs, J.-N. & Montambaux, G. Orbital magnetism in coupled-bands models. *Phys. Rev. B* **91**, 085120 (2015).
- [45] Göbel, B., Mook, A., Henk, J. & Mertig, I. Magnetoelectric effect and orbital magnetization in skyrmion crystals: Detection and characterization of skyrmions. *Phys. Rev. B* **99**, 060406 (2019).
- [46] Go, D. & Lee, H.-W. Orbital torque: Torque generation by orbital current injection. *Phys. Rev. Res.* **2**, 013177 (2020).
- [47] Lee, D. *et al.* Orbital torque in magnetic bilayers. *Nature Comms.* **12**, 6710 (2021).
- [48] Johansson, A., Göbel, B., Henk, J., Bibes, M. & Mertig, I. Spin and orbital Edelstein effects in a two-dimensional electron gas: Theory and application to SrTiO₃ interfaces. *Phys. Rev. Res.* **3**, 013275 (2021).
- [49] El Hamdi, A. *et al.* Observation of the orbital inverse Rashba-Edelstein effect. *Nature Phys.* **19**, 1855–1860 (2023).
- [50] Zhang, S. & Yang, Z. Intrinsic spin and orbital angular momentum Hall effect. *Phys. Rev. Lett.* **94**, 066602 (2005).
- [51] Bernevig, B. A., Hughes, T. L. & Zhang, S.-C. Orbitronics: The intrinsic orbital current in *p*-doped silicon. *Phys. Rev. Lett.* **95**, 066601 (2005).
- [52] Kontani, H., Tanaka, T., Hirashima, D., Yamada, K. & Inoue, J. Giant intrinsic spin and orbital Hall effects in Sr₂MO₄ (*M*= Ru, Rh, Mo). *Phys. Rev. Lett.* **100**, 096601 (2008).
- [53] Tanaka, T. *et al.* Intrinsic spin Hall effect and orbital Hall effect in *4d* and *5d* transition metals. *Phys. Rev. B* **77**, 165117 (2008).
- [54] Kontani, H., Tanaka, T., Hirashima, D., Yamada, K. & Inoue, J. Giant orbital Hall effect in transition metals: Origin of large spin and anomalous Hall effects. *Phys. Rev. Lett.* **102**, 016601 (2009).
- [55] Go, D., Jo, D., Kim, C. & Lee, H.-W. Intrinsic spin and orbital Hall effects from orbital texture. *Phys. Rev. Lett.* **121**, 086602 (2018).
- [56] Go, D., Jo, D., Lee, H.-W., Kläui, M. & Mokrousov, Y. Orbitronics: Orbital currents in solids. *Europhys. Lett.* **135**, 37001 (2021).
- [57] Pezo, A., Ovalle, D. G. & Manchon, A. Orbital Hall effect in crystals: Interatomic versus intra-atomic contributions. *Phys. Rev. B* **106**, 104414 (2022).
- [58] Canonico, L. M., Cysne, T. P., Molina-Sanchez, A., Muniz, R. & Rappoport, T. G. Orbital Hall insulating phase in transition metal dichalcogenide monolayers. *Phys. Rev. B* **101**, 161409 (2020).
- [59] Cysne, T. P., Bhowal, S., Vignale, G. & Rappoport, T. G. Orbital Hall effect in bilayer transition metal dichalcogenides: From the intra-atomic approximation to the Bloch states orbital magnetic moment approach. *Phys. Rev. B* **105**, 195421 (2022).
- [60] Salemi, L. & Oppeneer, P. M. Theory of magnetic spin and orbital Hall and Nernst effects in bulk ferromagnets. *Phys. Rev. B* **106**, 024410 (2022).
- [61] Busch, O., Mertig, I. & Göbel, B. Orbital Hall effect and orbital edge states caused by *s* electrons. *Phys. Rev. Res.* **5**, 043052 (2023).
- [62] Choi, Y.-G. *et al.* Observation of the orbital Hall effect in a light metal Ti. *Nature* **619**, 52–56 (2023).
- [63] Cysne, T. P. *et al.* Disentangling orbital and valley Hall effects in bilayers of transition metal dichalcogenides. *Phys. Rev. Lett.*

- 126, 056601 (2021).
- [64] Barbosa, A. L., Canonico, L. M., Garía, J. H. & Rapoport, T. G. Orbital hall effect and topology on a two-dimensional triangular lattice: from bulk to edge. *arXiv preprint arXiv:2311.11715* (2023).
- [65] Seifert, T. S. *et al.* Time-domain observation of ballistic orbital-angular-momentum currents with giant relaxation length in tungsten. *Nature Nanotechnol.* **18**, 1132 (2023).
- [66] Busch, O., Ziolkowski, F., Göbel, B., Mertig, I. & Henk, J. Ultrafast orbital Hall effect in metallic nanoribbons. *Phys. Rev. Res.* **6**, 013208 (2024).
- [67] Göbel, B. & Mertig, I. Orbital Hall Effect Accompanying Quantum Hall Effect: Landau Levels Cause Orbital Polarized Edge Currents. *Phys. Rev. Lett.* **133**, 146301 (2024).
- [68] Dias, M. d. S., Bouaziz, J., Bouhassoune, M., Blügel, S. & Lounis, S. Chirality-driven orbital magnetic moments as a new probe for topological magnetic structures. *Nature Comms.* **7**, 13613 (2016).
- [69] Lux, F. R., Freimuth, F., Blügel, S. & Mokrousov, Y. Engineering chiral and topological orbital magnetism of domain walls and skyrmions. *Commun. Phys.* **1**, 60 (2018).
- [70] Nayak, A. K. *et al.* Magnetic antiskyrmions above room temperature in tetragonal Heusler materials. *Nature* **548**, 561 (2017).
- [71] Peng, L. *et al.* Controlled transformation of skyrmions and antiskyrmions in a non-centrosymmetric magnet. *Nature Nanotechnol.* **15**, 181–186 (2020).
- [72] Jena, J. *et al.* Elliptical bloch skyrmion chiral twins in an antiskyrmion system. *Nature Comms.* **11**, 1115 (2020).
- [73] Jena, J. *et al.* Evolution and competition between chiral spin textures in nanostripes with D_{2d} symmetry. *Sci. Adv.* **6**, eabc0723 (2020).
- [74] Göbel, B. & Mertig, I. Quaternary-digital data storage based on magnetic bubbles in anisotropic materials. *Phys. Rev. Appl.* **15**, 064052 (2021).
- [75] Zhang, X. *et al.* Control and manipulation of a magnetic skyrmionium in nanostructures. *Phys. Rev. B* **94**, 094420 (2016).
- [76] Zhang, S., Kronast, F., van der Laan, G. & Hesjedal, T. Real-space observation of skyrmionium in a ferromagnet-magnetic topological insulator heterostructure. *Nano Letters* **18**, 1057–1063 (2018).
- [77] Göbel, B., Schäffer, A. F., Berakdar, J., Mertig, I. & Parkin, S. S. Electrical writing, deleting, reading, and moving of magnetic skyrmioniums in a racetrack device. *Sci. Rep.* **9**, 12119 (2019).
- [78] Kharkov, Y., Sushkov, O. & Mostovoy, M. Bound states of skyrmions and merons near the Lifshitz point. *Phys. Rev. Lett.* **119**, 207201 (2017).
- [79] Göbel, B., Mook, A., Henk, J., Mertig, I. & Tretiakov, O. A. Magnetic bimerons as skyrmion analogues in in-plane magnets. *Phys. Rev. B* **99**, 060407 (2019).
- [80] Gao, N. *et al.* Creation and annihilation of topological meron pairs in in-plane magnetized films. *Nature Comms.* **10**, 5603 (2019).
- [81] Yu, X. *et al.* Biskyrmion states and their current-driven motion in a layered manganite. *Nature Comms.* **5**, 3198 (2014).
- [82] Göbel, B., Henk, J. & Mertig, I. Forming individual magnetic biskyrmions by merging two skyrmions in a centrosymmetric nanodisk. *Sci. Rep.* **9**, 9521 (2019).
- [83] Nagaosa, N., Sinova, J., Onoda, S., MacDonald, A. H. & Ong, N. P. Anomalous Hall effect. *Rev. Mod. Phys.* **82**, 1539 (2010).